International Journal of Nanomedicine

Dovepress
open access to scientific and medical research

Open Access Full Text Article

ORIGINAL RESEARCH

Exosomes Derived from Bone Mesenchymal Stem Cells with the Stimulation of Fe_3O_4 Nanoparticles and Static Magnetic Field Enhance Wound Healing Through Upregulated miR-21-5p

This article was published in the following Dove Press journal:
International Journal of Nanomedicine

Di Wu[1]
Lin Kang[2]
Jingjing Tian[2]
Yuanhao Wu[2]
Jieying Liu[2]
Zhengyao Li[1]
Xiangdong Wu[1]
Yue Huang[1]
Bo Gao[3]
Hai Wang[1]
Zhihong Wu[2,4]
Guixing Qiu[1]

[1]Department of Orthopaedic Surgery, Peking Union Medical College Hospital, Peking Union Medical College and Chinese Academy of Medical Sciences, Beijing 100730, People's Republic of China; [2]Medical Science Research Center (MRC), Peking Union Medical College Hospital, Peking Union Medical College and Chinese Academy of Medical Sciences, Beijing 100730, People's Republic of China; [3]Umibio (Shanghai) Co. Ltd, Shanghai 201210, People's Republic of China; [4]Beijing Key Laboratory for Genetic Research of Bone and Joint Disease, Beijing 100730, People's Republic of China

Correspondence: Hai Wang
Department of Orthopaedic Surgery, Peking Union Medical College Hospital, Peking Union Medical College and Chinese Academy of Medical Sciences, No. 1 Shuaifuyuan, Beijing 100730, People's Republic of China
Email wanghai907@hotmail.com

Zhihong Wu
Medical Science Research Center (MRC), Peking Union Medical College Hospital, Peking Union Medical College and Chinese Academy of Medical Sciences, No. 1 Shuaifuyuan, Beijing 100730, People's Republic of China
Email wuzh3000@126.com

Background: Both magnetic nanoparticles (MNPs) and exosomes derived from bone mesenchymal stem cells (BMSC-Exos) have been reported to improve wound healing. In this study, novel exosomes (mag-BMSC-Exos) would be fabricated from BMSCs with the stimulation of MNPs and a static magnetic field (SMF) to further enhance wound repair.

Methods: Mag-BMSC-Exos, namely, exosomes derived from BMSCs preconditioned with Fe_3O_4 nanoparticles and a SMF, together with BMSC-Exos were both first isolated by ultracentrifugation, respectively. Afterwards, we conducted in vitro experiments, including scratch wound assays, transwell assays, and tube formation assays, and established an in vivo wound healing model. The miRNA expression profiles were compared between BMSC-Exos and mag-BMSC-Exos to detect the potential mechanism of improving wound healing. At last, the function of exosomal miR-21-5p during wound healing was confirmed by utilizing a series of gain- and loss-of-function experiments in vitro.

Results: The optimal working magnetic condition was 50 μg/mL Fe_3O_4 nanoparticles combined with 100 mT SMF. In vitro, mag-BMSC-Exo administration promoted proliferation, migration and angiogenesis to a greater extent than BMSC-Exo administration. Local transplantation of mag-BMSC-Exos into rat skin wounds resulted in accelerated wound closure, narrower scar widths and enhanced angiogenesis compared with BMSC-Exo transplantation. Notably, miR-21-5p was found to be highly enriched in mag-BMSC-Exos and served as a critical mediator in mag-BMSC-Exo-induced regulatory effects through inhibition of SPRY2 and activation of the PI3K/AKT and ERK1/2 signaling pathways.

Conclusion: Mag-BMSC-Exos can further enhance wound healing than BMSC-Exos by improving angiogenesis and fibroblast function, and miR-21-5p upregulation in mag-BMSC-Exos might be the potential mechanism. This work offers an effective and promising protocol to improve wound healing in clinic.

Keywords: exosomes, wound healing, miR-21-5p, angiogenesis, fibroblast function

Introduction

The skin, consisting of an outer epidermal layer and an inner dermal layer, play a key role in shielding internal tissues from mechanical damage, microbial infection, ultraviolet radiation, and extreme temperature.[1,2] The healing of skin wounds requires a well-orchestrated integration of cell migration and proliferation, collagen synthesis and deposition, angiogenesis, re-epithelialization and wound remodeling.[3,4] Patients

with diabetes, the elderly, and patients with very large surface wounds are especially predisposed to abnormal wound healing leading to long-term sequelae.[5] Thus, it is very important to improve wound healing and recover the barrier function of skin.

Stem cells are an attractive potential therapeutic agent for promoting cutaneous wound healing and have several distinct advantages, such as no risk to donors, easy accessibility, and a low incidence of graft-versus-host disease.[6,7] However, the direct use of stem cells for therapeutic purposes remains limited by many risk factors, such as tumor formation, thrombosis, and unwanted immune responses.[8,9] Exosomes are 50–150 nm-sized small membrane vesicles of endosomal origin that play crucial roles in intercellular communication by delivering miRNAs, mRNAs and proteins to recipient cells.[10,11] Treatment of exosomes from stem cells, which exhibit stem cell-like pro-regenerative properties, can overcome the previous described limitations of stem cell transplantation therapy.[12] Additionally, exosomes from stem cells can accelerate wound healing by promoting angiogenesis and fibroblast function.[13] Recently, magnetic nanoparticles (MNPs), such as Fe_3O_4 nanoparticles and γ-Fe_2O_3 nanoparticles, have drawn more and more attentions for their potentials in tissue regeneration.[14] They can impart continuous weak magnetic force on cells to improve tissue regeneration with a static magnetic field (SMF).[15] Additionally, the combination of MNPs and SMF can further enhance the wound healing process by modulating the phenotypic polarization of fibroblasts.[16]

Therefore, we sought to fabricate novel exosomes derived from bone mesenchymal stem cells (BMSCs) by stimulating with Fe_3O_4 nanoparticles and SMF (mag-BMSC-Exos), in order to improve the effect of exosomes derived from BMSCs (BMSC-Exos) for wound healing in this study. Meanwhile, the potential mechanisms of their promotion for wound healing would also be assessed by in vitro and in vivo experiments.

Materials and Methods

Cell Culture

Human BMSCs were obtained from American Type Culture Collection (ATCC; Manassas, VA, USA). BMSCs were cultured in basal medium (HUXMA-90011, Cyagen, Santa Clara, CA, USA) with 10% fetal bovine serum (FBS), 1% penicillin-streptomycin, and glutamine at 37 °C in saturated humidity at 5% CO_2. Early passage BMSCs (passages 3–5) were used for the in vitro study. The human umbilical vein endothelial cells (HUVECs), human skin fibroblasts (HSFs) and HEK-293 cells used in our present study were obtained from the cell bank of the Chinese Academy of Medical Sciences (Beijing, China). HUVECs and HSFs were cultured in high-glucose Dulbecco's modified Eagle medium (DMEM, Gibco BRL, Grand Island, USA) with 10% FBS and 1% penicillin-streptomycin. All cells were passaged every 2–3 days when they reached approximately 90% confluence.

Preparation of Fe_3O_4 and the SMF

A total of 20 mg Fe_3O_4 (Nanjing Nanoeast Biotech, Jiangsu, China) powder was soaked in 50 mL basal medium (400 μg/mL) and shaken at 37 °C for 24 h. The size of Fe_3O_4 was 100 nm, with high magnetic responsiveness and uniform particle size distribution. Also it is biocompatible and water solubile. Then, the basal medium containing Fe_3O_4 was diluted two-fold up to 1/16 (200, 100, 50 and 25 μg/mL). According to the cell viability of BMSCs treated with different concentrations of Fe_3O_4 nanoparticles, we chose the optimal concentration.

To investigate the effect of the SMF, BMSCs preconditioned with the optimal concentration of Fe_3O_4 were cultured under a SMF or no SMF environment. In the SMF group, three subgroups, SMF_{50}, SMF_{100}, and SMF_{150}, were tested using different magnetic field strengths (50, 100, and 150 mT, respectively). In brief, magnetic sheets (1 mm thick x 15 mm in diameter; Shenzhen Strong Magnets, Guangdong, China) were placed below the wells to expose the cultures to a north magnetic field. The desired field intensities were established by controlling the distance between the magnet and the culture dishes. A Gauss meter (TM-701, Kanetec, Tokyo, Japan) was used to measure the SMF intensity. According to the cell viability of BMSCs treated with optimal concentration of Fe_3O_4 and different magnetic strengths of SMF, the optimum magnetic condition was chosen. Then we used this optimum magnetic condition to stimulate BMSCs, and two types of cultural supernatants were used for the isolation of exosomes derived from BMSCs and BMSCs exposed to a magnetic environment (Fe_3O_4 nanoparticles and SMF).

Cell Proliferation Assay

The proliferation of BMSCs in response to Fe_3O_4 nanoparticles and SMF was measured by the Cell Counting

Kit-8 assay (CCK-8; Dojindo, Tokyo, Japan). Briefly, 5×10^3 cells/well (four replicates per group) were seeded into 96-well plates and then treated with different concentrations of Fe_3O_4 nanoparticles (400, 200, 100, 50 and 25 μg/mL). A group without nanoparticles served as the control. After culturing for 1, 3, and 5 days, CCK-8 solution (10 μL) and 90 μL of culture medium were added to each well and incubated at 37 °C for 1 h. The absorbance was observed at 450 nm by using a microplate reader (Varioskan Flash, Thermo Scientific™, USA), and the optical density was recorded for cell viability. Then, we cultured the BMSCs at the optimal concentration of Fe_3O_4 nanoparticles combined with different SMF strengths (50, 100, 150 mT), to measure cell viability as above.

The nanoscale morphology of the Fe_3O_4 nanoparticles taken up by BMSCs was observed by transmission electron microscopy (TEM) (Hitachi, Tokyo, Japan). According to the results of cell viability, we selected the best synergistic magnetic environment (concentration of Fe_3O_4 nanoparticles and strength of SMF) to stimulate the secretion of mag-BMSC-Exos.

Exosome Isolation

When BMSCs reached 70−80% confluence, they were washed and incubated for another 48 h in complete medium supplemented with 10% exosome-depleted FBS (Umibio, Shanghai, China). The cellular supernatant was collected and subjected to a series of low-speed centrifugation steps (300 ×g for 10 min, 2000 ×g for 20 min) to discard the cell debris. The exosome suspension was filtered through a 0.22 μm filter (Merck-Millipore, Darmstadt, Germany) to remove the residual cellular debris. Next, the supernatant was centrifuged at 10,000 ×g for 30 min followed by ultracentrifugation for 70 min at 100,000 ×g. The pelleted exosomes were washed twice with a large volume of PBS and centrifuged at 100,000 ×g for 70 min. Then, the exosomes at the bottom of the tube were resuspended in PBS. All procedures were performed at 4 °C. Exosomes were stored at –80 °C or used in further experiments.

Identification of Exosomes

The size distribution of exosomes was measured by nanoparticle tracking analysis (NTA) with a NanoSight NS500 instrument (Malvern Instruments, Malvern, UK). Then, the exosome size was analyzed using NTA software version 3.0 (Malvern), and the exosome morphologies were observed with TEM as described previously in detail.[13] Western blotting was used to determine the presence of specific exosomal surface markers, such as CD9, CD63, CD81 and TSG101. The residual Fe_3O_4 nanoparticles in mag-BMSC-Exos were evaluated based on the concentration of Fe by inductively coupled plasma (ICP; Varian, Palo Alto, CA, USA).

Exosome Internalization

To determine exosome uptake by HUVECs and HSFs, exosomes were labeled with the red fluorescent dye PKH26 (Sigma-Aldrich, St. Louis, MO, USA) according to the manufacturer's protocol[17] and then incubated with HUVECs and HSFs at 37 °C. At 4, 8, 12, 16 and 24 h, the cells were fixed in 4% paraformaldehyde for 15 min and then blocked with PBS containing 1% BSA for 20–30 min, followed by staining with PKH26 in PBS for 20 min at room temperature. The nuclei were dyed with DAPI (0.5 μg/mL; Invitrogen, Carlsbad, CA, USA) for 10 min, and the specimens were observed by confocal microscopy (Nikon, Tokyo, Japan). Then, the fluorescence intensity of PKH26 was measured at different time points in each group.

Migration Assay

For the scratch wound assay, HUVECs were cultured on 6-well plates at a density of 1×10^5 cells per well and incubated to reach confluence. The monolayer was scratched using 200 μL pipette tips and washed with PBS to remove detached cells. Then, the cells were cultured in serum-free medium with negative control (PBS, 200 μL/well), BMSC-Exos (100 μg/mL, 200 μL/well) or mag-BMSC-Exos (100 μg/mL, 200 μL/well). HUVECs were imaged 0 and 24 h later. The wound closure area was calculated as follows: migration area (%) = $(A_0 - An)/A_0 \times 100\%$, where A_0 represents the area of the initial wound and An represents the remaining area of the wound at the measurement point.

For the transwell assay, 1×10^4 cells/well were suspended in serum-free medium and seeded into the upper chamber of 24-well transwell plates (Corning, NY, USA) with 8 μm pore filters. Then the lower chamber was filled with DMEM supplemented with 10% exosome-depleted FBS and mixed with negative control (PBS, 200 μL/well), BMSC-Exos (100 μg/mL, 200 μL/well) or mag-BMSC-Exos (100 μg/mL, 200 μL/well). After incubation at 37 °C for 24 h, the cells attached to the upper surface of the filter membranes were removed, and the migrated cells on the lower surface were stained with 0.1% crystal violet for

several minutes. The level of migration was observed under an optical microscope (Leica, Solms, Germany). The transwell assay of HSFs followed the same protocol as the one with HUVECs. All experiments were performed in triplicate.

Tube Formation Assay

The in vitro angiogenesis assay was conducted using the Matrigel basement membrane matrix (356234, BD Biosciences, San Jose, USA) according to the manufacturer's instructions. Briefly, the Matrigel was thawed overnight at 4 °C. Then, Matrigel was added to 96-well plates at 50 μL per well using cold tips on ice and incubated at 37°C to solidify. Next, 2×10^4 HUVECs/well were resuspended in complete medium supplemented with 10% exosome-depleted FBS and treated with negative control (PBS, 10 μL/well), BMSC-Exos (100 μg/mL, 10 μL/well), or mag-BMSC-Exos (100 μg/mL, 10 μL/well). After incubation at 37 °C for 6 h, tube formation was observed by an inverted microscope. The total tube length was carefully measured by randomly selecting five fields per well using ImageJ software (Media Cybernetics, Bethesda, USA).

qRT-PCR Analysis

Total RNA was extracted from cells and exosomes using TRIzol Reagent (Invitrogen, Carlsbad, CA, USA). For mRNA detection, cDNA was synthesized from 1 μg of total RNA by using a Revert Aid first-strand cDNA synthesis kit (Takara, Shiga, Japan). For the miRNA analysis, exosomal miRNAs were isolated by using the Exosome RNA Purification Kit (Umibio, Shanghai, China), and cDNA of miRNAs was synthesized using the SYBR Green microRNA assay kit (Applied Biosystems, Foster City, USA) as described by the manufacturer's protocol. All real-time PCR was performed on the ABI PRISM® 7900HT System using the SYBR Green-based real-time detection method. The relative standard curve method ($2^{-\Delta\Delta CT}$) was used to determine the relative mRNA and miRNA levels in cells, using GAPDH or U6 as the housekeeping gene, respectively. miRNA levels in exosomes were normalized with cel-miR-39 levels (Exiqon, Vedbaek, Denmark). The PCR primer sequences used in this study are listed in Supplementary Table 1.

Western Blotting

The total protein concentrations in cells and exosomes were determined using a BCA protein assay kit (Thermo Scientific, Waltham, MA, USA). The cells and exosomes were lysed in RIPA lysis buffer (Millipore Corporation, Billerica, MA, USA), and equal amounts of protein were separated by SDS-PAGE gels and transferred to PVDF membranes (Merck Millipore, MA, USA). Blots were blocked with 5% milk in Tris-buffered saline containing 0.1% Tween-20 for 1 h at room temperature. The membranes were incubated with primary antibodies at 4 °C overnight, followed by incubation with HRP-linked secondary antibodies at 37 °C for 1 h. Antibodies against the exosomal markers CD9, CD63, CD81, and TSG101 and the negative marker calnexin were obtained from Abcam (1:1000; Abcam, Cambridge, UK); antibodies against ANG-1, VEGF, HIF-1α, bFGF, PDGFRα, GAPDH, β-actin, AKT, p-AKT, ERK1/2, and p-ERK1/2 were obtained from Cell Signaling Technology (1:1000; Beverly, MA, USA). The immunoreactive bands were visualized using enhanced chemiluminescence reagent (Thermo Fisher Scientific, Waltham, USA) and quantified using ImageJ software.

Rat Skin Wound Model and Treatment

All experimental procedures were approved by the ethics committee of the Peking Union Medical College Hospital (XHDW-2020-043). The Guide for the Care and Use of Laboratory Animals (GB14925-2010; NIH), and the Laboratory Animal Center of Peking Union Medical College Hospital were strictly adhered to. Six-week-old male SD rats (weighing 300–400 g) were used in this study. The rats were anesthetized by intraperitoneal administration of 50 mg/kg pentobarbital sodium (Sigma-Aldrich, St. Louis, MO, USA) before surgery. After shaving the rats, a full-thickness excisional skin wound (20 mm×20 mm) was created on the dorsum. Twenty-four rats were randomly divided into three treatment groups, which were subcutaneously injected with 100 μL PBS, BMSC-Exos (100 μg dissolved in 100 μL PBS), and mag-BMSC-Exos (100 μg dissolved in 100 μL PBS) around the wounds at 4 injection sites (25 μL per site, Figure S1). Fourteen days after the operation, the rats were sacrificed, and skin specimens were harvested.

The wounds of each group were imaged at 0, 4, 7, 10 and 14 days after surgery. All wounds were measured with a right-angle ruler, and the area of each wound was evaluated using ImageJ software. The reduction in wound size was calculated as follows: wound size reduction (%) = $(A_0 - A_t)/A_0 \times 100\%$, where A_0 is the initial wound area, and A_t is the wound area at days 4, 7, 10 or 14 post surgery.

Microfil Perfusion and Microcomputed Tomography

Microfil@ contrast agent (MV122; Flow Tech, VA, USA) was prepared according to the manufacturer's instructions. Briefly, the hair on the chest was shaved, and the rib cage was opened with a pair of scissors. Then, 100 mL of heparinized saline and 20 mL of Microfil was continuously perfused at a rate of 2 mL/min. After the contrast agent was perfused, the abdominal aorta and inferior vena cava were closed by ligation, and the animals were stored at 4 °C overnight. Then, specimens were fixed in 4% paraformaldehyde, followed by micro-CT evaluation of vascularization. Subsequently, 3D reconstruction was performed for qualitative analysis.

Histological and Immunofluorescence Analysis

The collected rat specimens containing the wound bed and surrounding healthy skin were processed for further investigation. The tissues were fixed in 4% paraformaldehyde solution, dehydrated with a series of graded ethanol solutions and embedded in paraffin. Sections (5 μm thick) were stained with hematoxylin and eosin (H&E) and imaged under an optical microscope. Masson's trichrome staining was used to evaluate the degree of collagen maturity.

For the immunohistochemical analysis, the sections were rehydrated, blocked, and incubated with primary anti-CD31 antibody (1:100; Abcam, Cambridge, UK) at 4 °C overnight. After incubation with the secondary antibody (1:250; Abcam, Cambridge, UK) at room temperature, the stained sections were visualized using the DAB substrate and finally counterstained using hematoxylin. Immunofluorescence staining for CD31 was performed to estimate the extent of newly formed capillaries. Sections were incubated with the anti-CD31 antibody overnight at 4 °C and then with the Cy3-conjugated secondary antibody at room temperature for 1 h away from light. To compare the number of blood vessels from different groups, five random fields per section near the wound edges were counted by using ImageJ software.

Bioinformatics Analysis

The miRNA expression profiles of BMSC-Exos and mag-BMSC-Exos were determined by small RNA sequencing. Briefly, total RNA was extracted from exosomes and ligated with 3′ and 5′ end adapters. PCR was performed to synthesize first-strand cDNA and for amplification. Then, the PCR products were purified, and sequencing was performed on an Illumina HiSeq 3000 platform. The expression levels of miRNAs were estimated by comparing the sequencing data to a bioinformatics miRNA database and corrected by the number of reads per million. Target genes of miRNAs were predicted by the online tools TargetScan, miRDB, miRTarBase, and miRWalk. Candidate target genes were determined based on prediction results from multiple software programs. Kyoto Encyclopedia of Genes and Genomes (KEGG) pathway enrichment analysis was performed for candidate target genes whose functions were linked with angiogenesis and fibrogenesis.

Luciferase Reporter Assay

The wild-type and mutant 3′-UTRs of SPRY2 were amplified by polymerase chain reaction (PCR) and inserted into the pGL3 plasmid. HEK293 cells (1×10^4) were seeded in 48-well plates and cotransfected with the wild-type or mutant luciferase reporter (100 ng) and miR-21-5p mimic (20 nM) or negative controls using Lipofectamine 3000 (Invitrogen, CA, USA) as indicated. After 48 h, the relative luciferase activity was detected by a luciferase reporter system (Promega, Madison, USA).

MiRNA Transfection and SPRY2 Inhibition/Overexpression

MiR-21-5p mimic, miR-21-5p inhibitor and their negative controls were purchased from RiboBio (Guangzhou, China). Briefly, the cells were cultured in 6-well culture plates and transfected with miR-21-5p mimic, miR-21-5p inhibitor or their negative controls using Lipofectamine 3000. After 48 h of incubation, subsequent experiments were performed.

To assess whether SPRY2 knockdown can achieve similar effects on angiogenesis and fibroblast function as miR-21-5p, SPRY2 siRNA obtained from RiboBio (Guangzhou, China) was used to knock down the expression of SPRY2 in HUVECs and HSFs. Briefly, cells were transfected with si-SPRY2 or negative control siRNA (si-NC) using Lipofectamine 3000 according to the manufacturer's instructions. Forty-eight hours later, the knockdown efficiency was verified by qRT-PCR. The sequences of si-SPRY2 were as follows: forward: 5′-AUAAACAAGGCAAAAAGAGGG-3′ and reverse: 5′-CUCUUUUUGCCUUGUUUAUGG-3′. Overexpression of SPRY2 was achieved by transfecting

SPRY2 cDNA (Wei Zheng, Shandong, China) and using Lipofectamine 3000.

Statistical Analysis

All experiments were performed with at least three replicates per group. Data are representative of these experiments and are shown as the means ± standard deviation (SD). Two treatment groups were compared by Student's *t*-test. Multiple group comparisons were performed by two-way analysis of variance with Tukey's post hoc test. Statistical analysis was conducted using GraphPad Prism 7.0 software, and statistical significance was declared as (*) $p < 0.05$, (**) $p < 0.01$ and (***) $p < 0.001$.

Results

Magnetic Environment Characterizations

To analyze the optimal working concentration of Fe_3O_4 nanoparticles and magnetic strength of SMF without impacting cell viability in our study, BMSCs were incubated with media at concentrations of 0, 25, 50, 100, 200 and 400 μg/mL Fe_3O_4 nanoparticles. The CCK-8 results showed that BMSCs treated with 50 μg/mL Fe_3O_4 nanoparticles had remarkably increased cell viability (Figure 1A). Similarly, BMSCs were cultured with media at the optimal working concentration of Fe_3O_4 nanoparticles (50 μg/mL) under different SMF strengths, and the CCK-8 results revealed that BMSCs treated with 50 μg/mL Fe_3O_4 nanoparticles combined with 100 mT magnetic field showed the most optimal cell viability (Figure 1B). The nanoscale morphology of the Fe_3O_4 nanoparticles taken up by BMSCs was observed by TEM, and the results revealed that these magnetic nanoparticles were swallowed by cells and distributed in the cell nucleus and cytoplasm (Figure 1C).

Isolation and Characterization of Exosomes

Next, we isolated, characterized and quantified exosomes derived from BMSCs and mag-BMSCs by using TEM analysis, NTA analysis and Western blotting. As shown in Figure 1D and E, TEM revealed that exosomes exhibited a cup- or sphere-shaped morphology, and NTA measurements showed that the diameters of these particles predominantly ranged from 50 to 150 nm (average 118.1 nm and 116.2 nm) in both the BMSC-Exo and mag-BMSC-Exo groups. No morphological difference between the two groups was observed with regard to their size, shape, or electron density. Moreover, the exosome concentration of the mag-BMSC-Exo group was significantly higher than that of the BMSC-Exo group (Figure S2, $P<0.001$). Western blotting analysis showed the presence of exosomal surface markers, including CD9, CD63, CD81 and TSG101 and the absence of negative control Calnexin (Figure 1F). The residual Fe_3O_4 nanoparticles in mag-BMSC-Exo was about 7.48nmol/mL (Fe:1256.71ng/mL).

The Differential Uptake of Exosomes by HUVECs and HSFs

To examine whether BMSC-Exos and mag-BMSC-Exos were differentially taken up by HUVECs and HSFs, PKH26 was used to label the exosomes, and the exosomes were then cocultured with HUVECs and HSFs for 24 h. Fluorescence microscopy was used to monitor the rate of exosome uptake by HUVECs and HSFs in real time. As shown in Figure 1G, the number of exosomes taken up by HUVECs and HSFs was significantly higher in the mag-BMSC-Exo group compared to the BMSC-Exo group. Figure 1H demonstrated a clear statistically significant difference between the two groups after 16 h ($P<0.05$) or 20 h ($P<0.001$), suggesting that mag-BMSC-Exos are taken up more easily by HUVECs and HSFs.

Exosomes Promote Proliferation, Migration, and Tube Formation in HUVECs and HSFs

To determine the activities of exosomes released from BMSCs and mag-BMSCs, we cultured HUVECs and HSFs in vitro with PBS, BMSC-Exos or mag-BMSC-Exos at a concentration of 100 μg/mL. Using scratch wound (Figure 2A and B) and transwell assays (Figure 2C and D), we found that both BMSC-Exos and mag-BMSC-Exos increased the migration of HUVECs when compared to the PBS group. Furthermore, as shown in Figure 2E and F, both BMSC-Exos and mag-BMSC-Exos significantly enhanced tube formation compared to the PBS group, as evidenced by an increased tube length ($P<0.001$). However, mag-BMSC-Exo treatment greatly enhanced the migration and tube formation capability of HUVECs compared to BMSC-Exos alone ($P<0.01$). Similarly, both BMSC-Exos and mag-BMSC-Exos increased the migration rate of HSFs (Figure 2G and H).

Next, we analyzed the expression levels of pro-angiogenic and pro-fibrogenic genes at both the mRNA and protein levels. The qRT-PCR results indicated that the

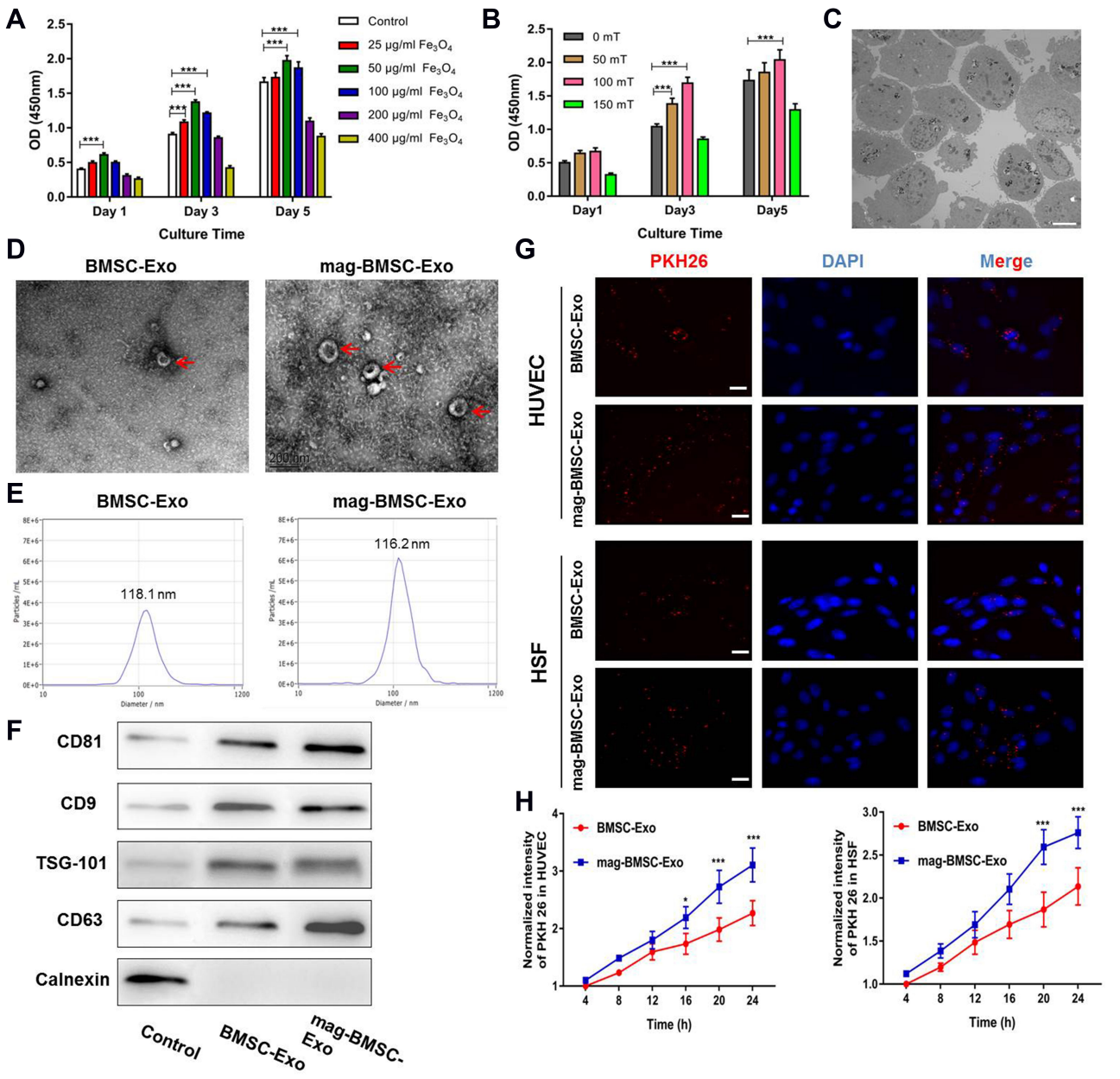

Figure 1 Magnetic stimulation promoted exosome release from BMSCs. (*) $p < 0.05$, (***) $p < 0.001$. (**A**) CCK-8 assay measuring the proliferation of BMSCs cultured in different concentrations of Fe_3O_4 nanoparticles. (**B**) Proliferation of BMSCs treated with the optimal working concentration (50 μg/mL) of Fe_3O_4 nanoparticles and exposed to different SMF strengths. (**C**) The internalization of Fe_3O_4 by BMSCs. Scale bar = 5μm. (**D**) Morphology of BMSC-Exos and mag-BMSC-Exos under TEM; the red arrows indicate exosomes. Scale bar = 200 nm. (**E**) NTA analysis of BMSC-Exos and mag-BMSC-Exos revealed that exosomes from the two groups exhibit similar size ranges (50–150 nm). (**F**) Western blotting analysis of the exosomal proteins CD9, CD63, CD81,TSG101 and negative control calnexin. (**G**) Uptake of red fluorescence dye PKH26-labeled BMSC-Exos and mag-BMSC-Exos by HUVECs and HSFs. Scale bar = 50 μm. (**H**) Statistical evaluation of fluorescence intensities at different times.

mRNA expression of VEGF, HIF-1α, PDGFRα and bFGF was substantially upregulated in the mag-BMSC-Exo and BMSC-Exo groups compared to the PBS group (Figure 2I–L). Similarly, the Western blotting assay confirmed that the protein expression levels of VEGF, HIF-1α, PDGFRα and bFGF were markedly increased after treatment with mag-BMSC-Exos and BMSC-Exos (Figure 2M). Collectively, these findings revealed that mag-BMSC-Exos and BMSC-Exos could promote a greater increase in proliferation, migration and tube formation compared to PBS treatment in vitro, simultaneously leading to the substantial upregulation of critical pro-angiogenic and pro-fibrogenic genes in vitro. More importantly, mag-BMSC-Exos had a greater effect than BMSC-Exos, which further proved that magnetic exosome-mediated angiogenesis and fibroblast function was mainly attributed to the combined effect of Fe_3O_4 and SMF.

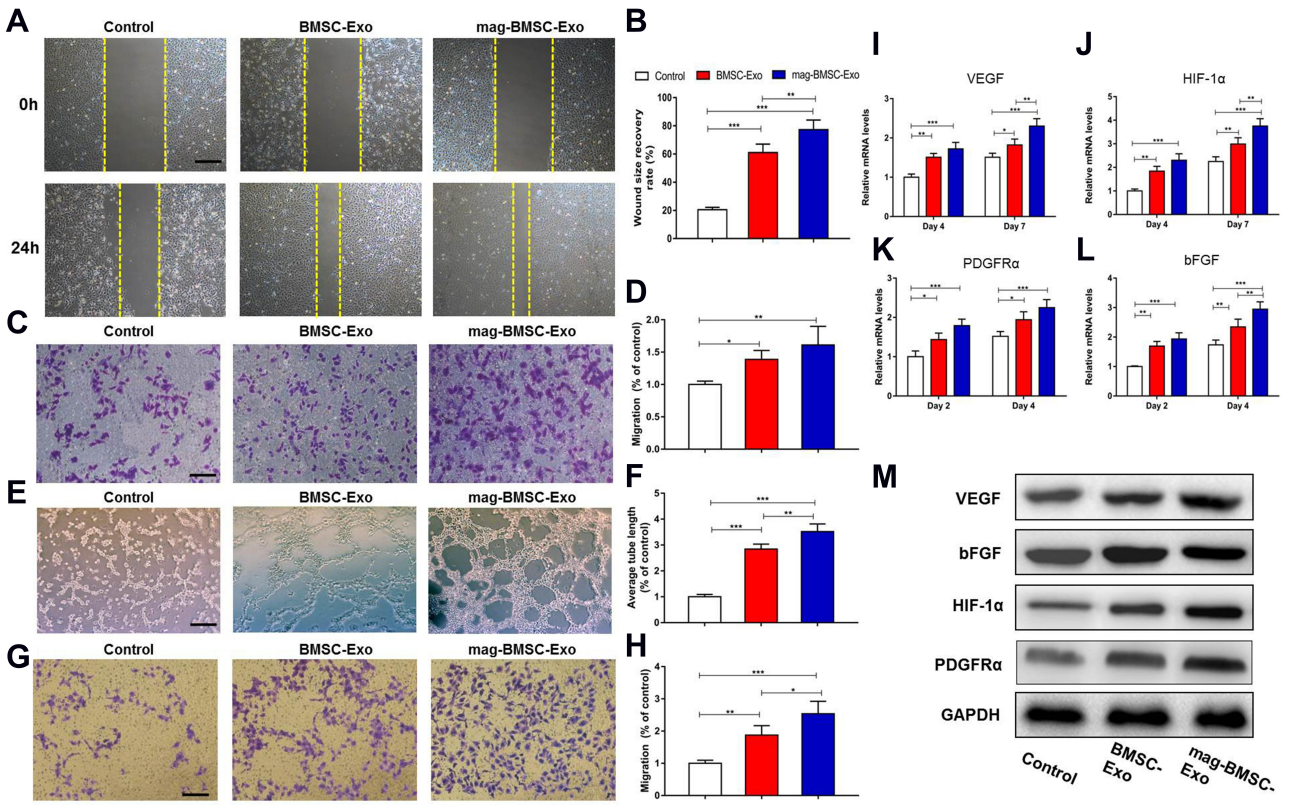

Figure 2 In vitro assay of cells treated with PBS, BMSC-Exos or mag-BMSC-Exos. (*) $p < 0.05$, (**) $p < 0.01$, (***) $p < 0.001$. (**A**) Representative images showing the migration ability of HUVECs at 24 h by scratch wound assay; the yellow dashed lines are the edges of the cell migration. Scale bar = 200 μm. (**B**) Quantitative analysis of the wound size recovery rate of HUVECs. (**C**) Representative images showing migrated HUVECs using the transwell assay. Scale bar = 200 μm. (**D**) Quantitative analysis of the migration rate of HUVECs. (**E**) Representative images showing tube formation in HUVECs. Scale bar = 200 μm. (**F**) Quantitative analysis of the tube formation assay. The values of the average tube length were measured. (**G**) Representative images showing migrated HSFs using the transwell assay. Scale bar = 200 μm. (**H**) Quantitative analysis of the migration rate of HSFs. (**I** and **J**) qRT-PCR analysis of the angiogenesis-related genes VEGF (**I**) and HIF-1α (**J**) at days 4 and 7. (**K** and **L**) qRT-PCR analysis of the fibrogenesis-related genes PDGFRα (**K**) and bFGF (**L**) at days 2 and 4. (**M**) Western blotting assay for the protein expression of VEGF, HIF-1α, PDGFRα and bFGF.

Exosomes Accelerate Cutaneous Wound Healing in Rats

To determine the effects of BMSC-Exos and mag-BMSC-Exos on cutaneous wound healing, we evaluated wound healing in three groups of animals that were treated with PBS, BMSC-Exos or mag-BMSC-Exos in and around the wound sites. Rats treated with mag-BMSC-Exos showed greater wound closure than rats in the PBS and BMSC-Exo groups at days 4, 7, 10 and 14 post wounding (Figure 3A). Microfil perfusion was performed to evaluate the blood vessels in the wound sites. The reconstructed 3D images after micro-CT scanning showed a significantly increased density of blood vessels after administration of mag-BMSC-Exos and BMSC-Exos compared to that in the PBS group (Figure 3B). As shown by H&E and Masson's trichrome staining (Figure 3C and D), treatment with both BMSC-Exos and mag-BMSC-Exos significantly enhanced re-epithelialization compared to that observed in the PBS group. The highest rate of wound closure, greatest degree of formation of blood vessels, narrowest scar widths and largest collagen deposition areas were observed in the mag-BMSC-Exo group at day 14 post wounding compared to the PBS and BMSC-Exo groups (Figure 3E–G). We also observed increased formation of sebaceous glands and hair follicles in the mag-BMSC-Exo and BMSC-Exo groups relative to the PBS group (Figure 3D). Vascularization of newly formed tissues is an essential step in the wound-healing process. Newly formed vessels at wound sites were characterized by immunohistochemical staining for CD31 (Figure 3H) and immunofluorescence staining for CD31 (Figure 3I), from which vessel densities were quantified (Figure S3). These data showed that the number of newly formed vessels increased during the healing process in all groups. The mag-BMSC-Exo group showed the highest vessel densities at day 14 compared with the control and BMSC-Exo groups.

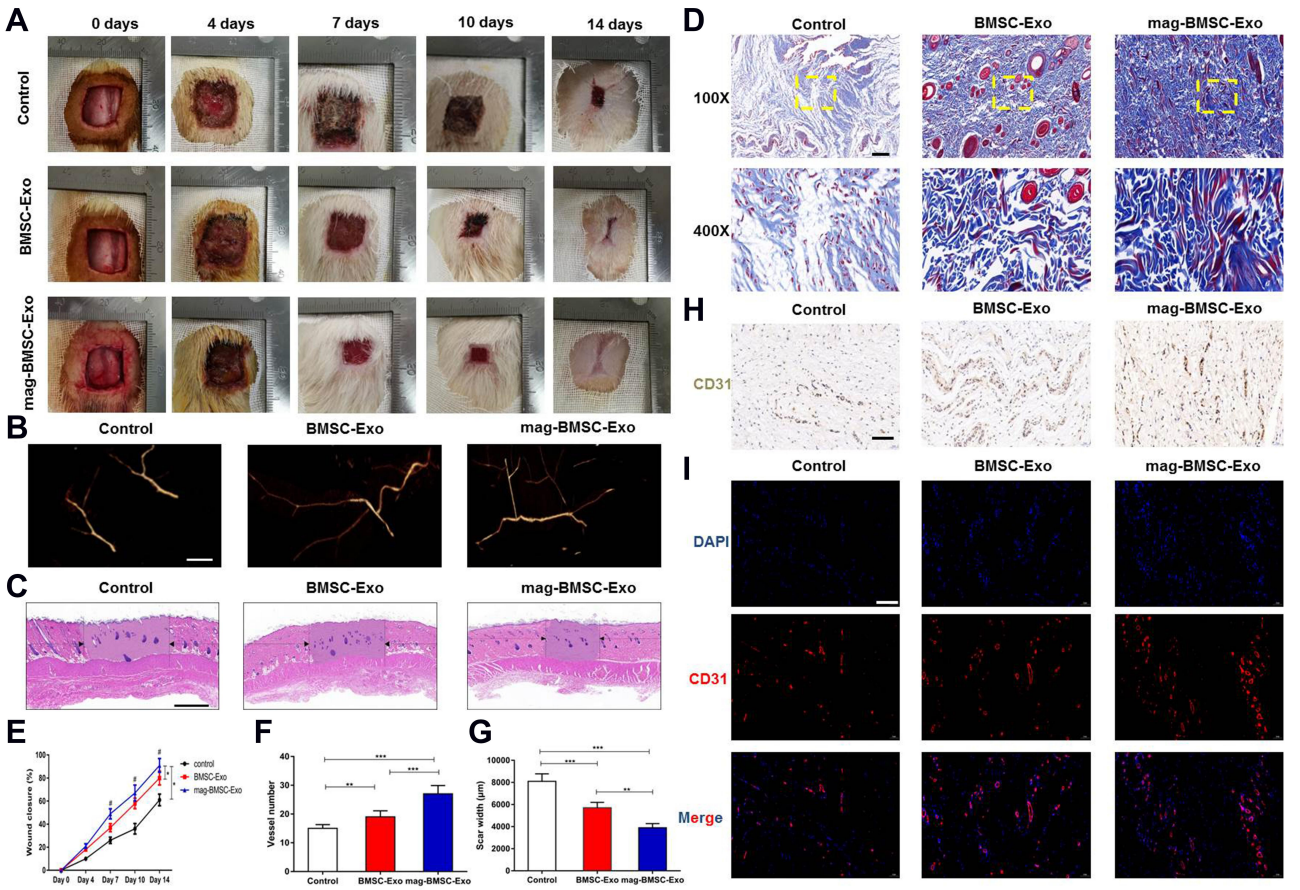

Figure 3 Mag-BMSC-Exos further accelerate cutaneous wound healing in rats. (*) $p < 0.05$, (**) $p < 0.01$, (***) $p < 0.001$. (**A**) Gross view of wounds treated with PBS, BMSC-Exos or mag-BMSC-Exos on days 0, 4, 7, 10 and 14 after wounding. (**B**) Microfil perfusion for determination of blood vessel density in the wound sites on day 14 after wounding. (**C**) H&E staining of wound sections from the three groups on day 14 after wounding. The black arrows indicate the edges of the scar. Scale bar = 1000 μm. (**D**) Masson's trichrome staining for the evaluation of collagen maturity; yellow dashed lines for the magnification. Scale bar = 100 μm (top) or 50 μm (bottom). (**E**) The wound closure rates of the three groups on days 0, 4, 7, 10 and 14 after wounding. ($^{\#}$) $p < 0.05$. (**F**) Quantitative analysis of the number of blood vessels in the three groups. (**G**) Quantitative analysis of the scar widths in the three groups. (**H**) Immunohistochemical staining of CD31 in wound sections on day 14 after wounding. Scale bar = 50 μm. (**I**) CD31 immunofluorescence staining of wound sections from the three groups on day 14 after wounding. Scale bar = 50 μm.

MiR-21-5p is Upregulated in Mag-BMSC-Exos and Transferred to HUVECs and HSFs by Exosomes

Both in vitro and in vivo analyses revealed that mag-BMSC-Exos enhanced angiogenesis compared to BMSC-Exos. It has been well recognized that miRNAs are one of the main functional components of exosomes and may play a crucial role in cell communication eventually regulating biological functions. We selected miR-21-5p as a candidate miRNA according to the miRNA sequencing data and KEGG pathway enrichment analysis, as well as based on reports in the literature showing that miR-21-5p not only enhances angiogenic activities but also promotes fibroblast proliferation, migration and collagen synthesis,[13,18,19] all of which are beneficial for wound healing (Figure 4A). As Figure 4B shows, miR-21-5p levels increased remarkably in mag-BMSC-Exos compared with BMSC-Exos ($P<0.001$). To confirm that mag-BMSC-Exo-secreted miR-21-5p can be transferred to HUVECs and HSFs via exosomes, we detected miR-21-5p levels in HUVECs and HSFs treated with mag-BMSC-Exos or BMSC-Exos. An increase in the cellular level of mature miR-21-5p, but not pri-/pre- miR-21, was observed in recipient HUVECs and HSFs following treatment with mag-BMSC-Exos (Figure 4C and D). In addition, the increase in miR-21-5p in HUVECs and HSFs exposed to mag-BMSC-Exos was not prevented by an RNA polymerase II inhibitor (Figure 4E). These data revealed that mag-BMSC-Exos containing miR-21-5p were internalized by HUVECs and HSFs.

MiR-21-5p Promotes Proliferation, Angiogenesis and Migration

We predicted possible miR-21-5p targets that contribute to angiogenic and fibrogenic functions by exploring online databases. To confirm the direct binding between miR-21-5p and

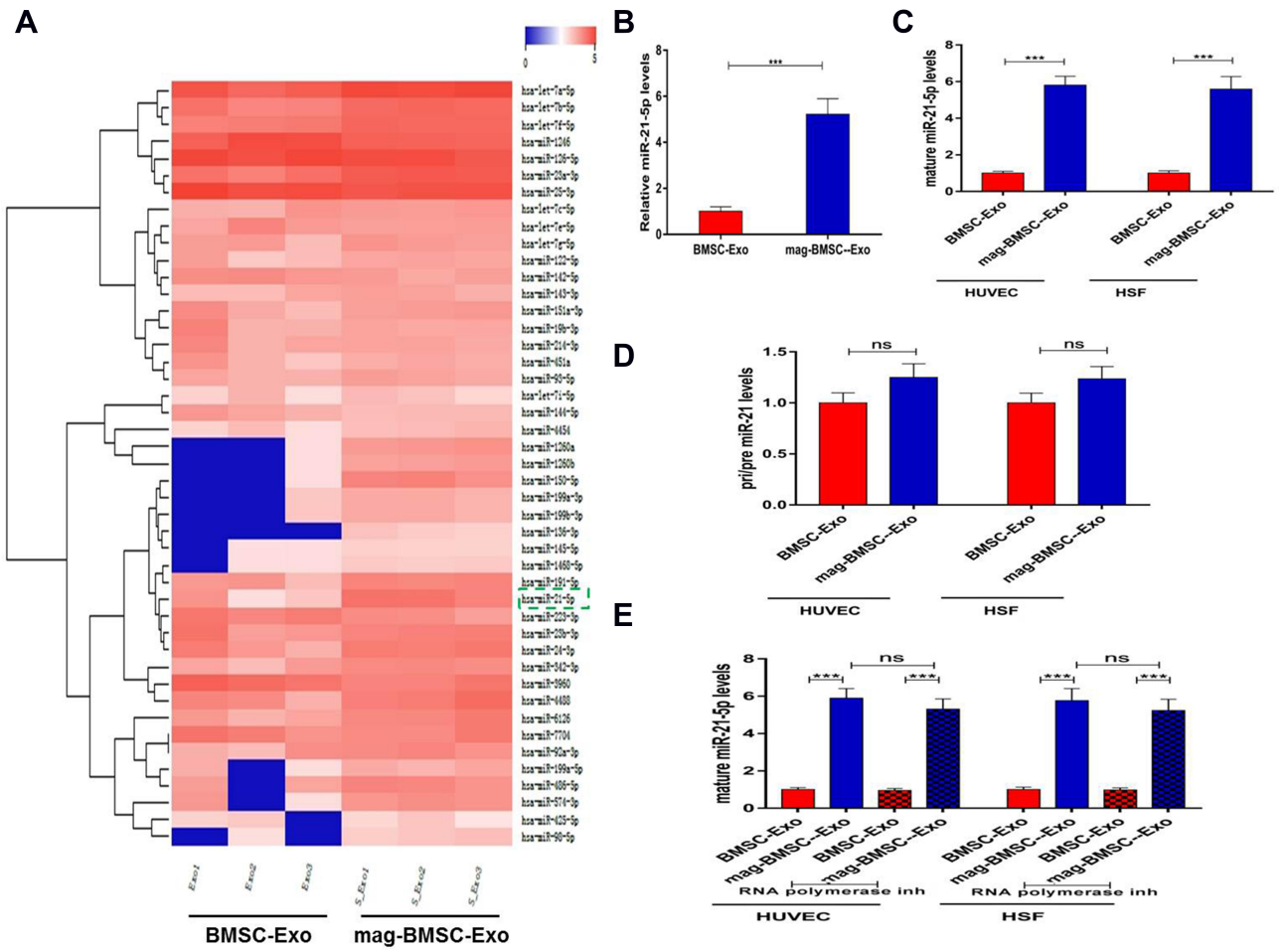

Figure 4 Upregulated miR-21-5p in mag-BMSC-Exos can be transferred to HUVECs and HSFs. (***) p < 0.001. (**A**) Heatmap of the miRNAs with a ≥2-fold difference between BMSC-Exos and mag-BMSC-Exos. Blue and red colors indicate downregulation and upregulation, respectively; green dashed lines indicate the selected miRNA. (**B**) qRT-PCR confirmation of the high level of miR-21-5p in mag-BMSC-Exos. (**C** and **D**) The levels of mature and pri/pre miR-21 in exosome-treated HUVECs and HSFs. (**E**) RNA polymerase II inhibitor did not change the level of miR-21-5p in HUVECs or HSFs exposed to mag-BMSC-Exos.
Abbreviations: WT, wild-type; MT, mutant; ns, no significance.

the 3′UTR of its predicted target gene SPRY2, we conducted a reporter assay using a luciferase reporter plasmid containing wild-type or mutated SPRY2 3′UTR with the miR-21-5p binding site (Figure 5A). MiR-21-5p mimic transfection reduced luciferase activity compared to control mimic transfection in HUVECs and HSFs (Figure 5B). Consistent with the results from the reporter assay, transfection with the miR-21-5p mimic resulted in a significant decrease in the level of SPRY2 in HUVECs and HSFs (P<0.001) (Figure 5C).

To verify that silencing SPRY2 had the same effect as miR-21-5p on proliferation, migration and angiogenesis, we transfected si-SPRY2 and si-NC into HUVECs and HSFs. In addition, miR-21-5p mimic and mimic-NC were administered. Given the known functions of SPRY2 as a negative regulator of endothelial cell proliferation, angiogenesis and migration, along with our gain- and loss-of function assay results, we confirmed that the miR-21-5p mimic and si-SPRY2 could both promote proliferation, angiogenesis and migration in HUVECs (Figure 5D, E, G and Figure S4A and S4B) and HSFs (Figure 5F, G and Figure S4C).

Studies have shown that miR-21 can target SPRY in HUVECs to induce the activation of the PI3K/AKT and ERK1/2 pathways, and the activation of the PI3K/AKT and ERK1/2 signaling pathways has been demonstrated to stimulate multiple critical steps in angiogenesis and fibroblast function.[13,20,21] To determine whether miR-21-5p could activate these signaling pathways, Western blotting was carried out to assess the protein levels of p-AKT and p-ERK1/2 in HSFs following treatment with mimic-NC or miR-21-5p mimic for 48 h. The cells were also treated with si-SPRY2 or si-NC as described above. Western blotting images revealed

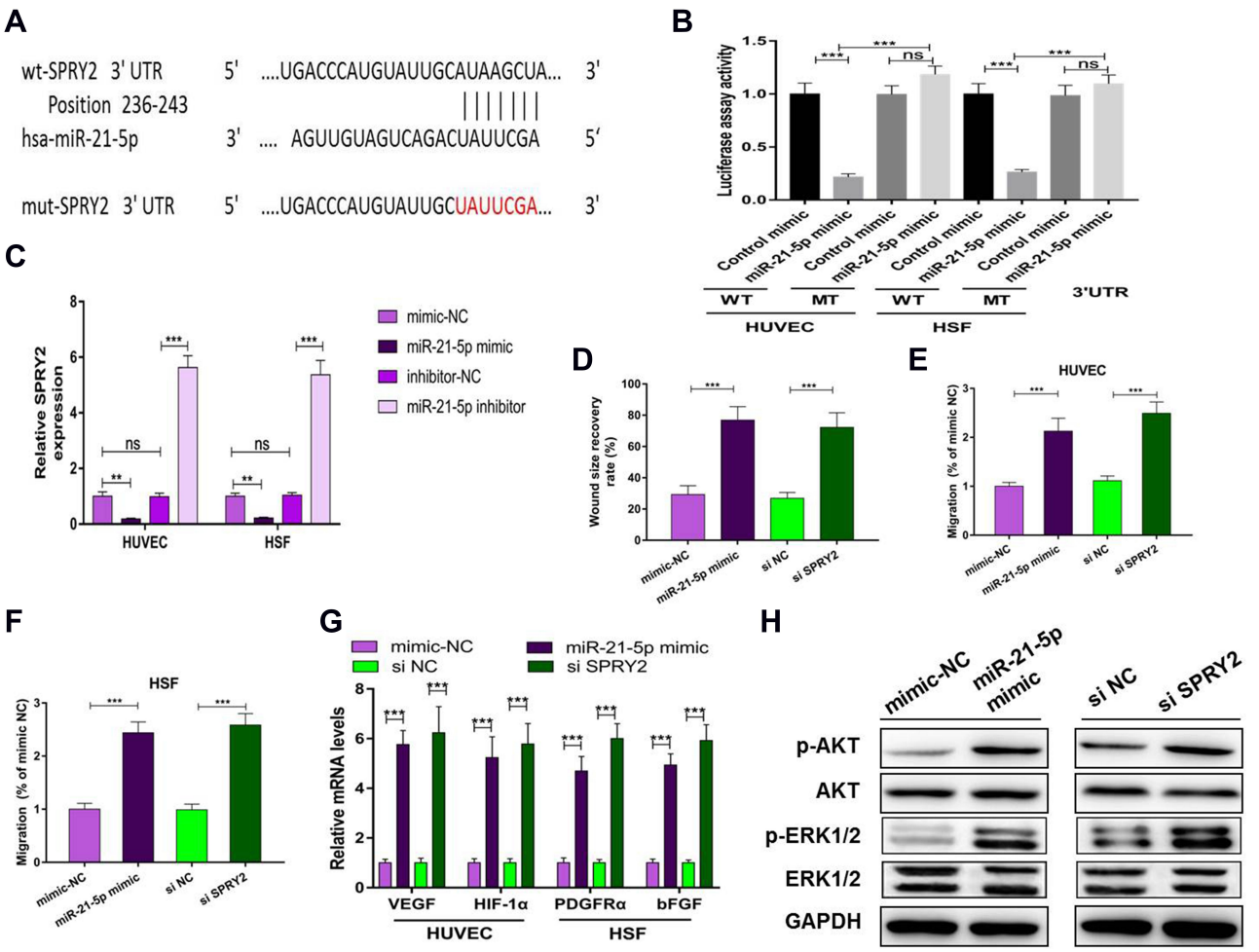

Figure 5 Exosomal miR-21-5p regulates SPRY2 by directly targeting the 3′-UTR. ns: no significance; (**) $p < 0.01$, (***) $p < 0.001$. (**A**) The miR-21-5p binding sequence in the 3′-UTR of SPRY2. (**B**) A luciferase reporter assay was performed to confirm that SPRY2 is the target gene of miR-21-5p. (**C**) mRNA level of SPRY2 in HUVECs and HSFs after transfection with miR-21-5p mimic or miR-21-5p inhibitor or their negative controls. (**D**) Quantitative analysis of the wound size recovery rate of HUVECs after transfection with miR-21-5p mimic or si SPRY2 or their negative controls. (**E** and **F**) Quantitative analysis of the migration rate of HUVECs and HSFs after transfection with miR-21-5p mimic, si SPRY2 or their negative controls. (**G**) qRT-PCR analysis of VEGF, HIF-1α, PDGFRα and bFGF after transfection with miR-21-5p mimic, si SPRY2 or their negative controls. (**H**) Western blotting assay for the protein expression of AKT, p-AKT, Erk1/2, p-Erk1/2, VEGF, HIF-1α, PDGFRα and bFGF after transfection with miR-21-5p mimic, si-SPRY2 or their negative controls.

that both the miR-21-5p mimic and si-SPRY2 induced significant increases in the phosphorylation of AKT and ERK1/2 (Figure 5H). These findings indicated that exosomal miR-21-5p of mag-BMSCs inhibited SPRY2 expression and increased angiogenesis and fibroblast function in HUVECs and HSFs.

Exosomal miR-21-5p Promotes Angiogenesis and Fibroblast Function by Targeting SPRY2 in vitro

To further explore the relationship between exosomal miR-21-5p and SPRY2, a series of in vitro rescue experiments were conducted. We transfected miR-21-5p mimic or miR-NC into HUVECs and HSFs and then cotransfected them with pcDNA-NC or pcDNA-SPRY2. As shown in Figure 6A–D, the effect of miR-21-5p mimic on promoting proliferation and migration in HUVECs and HSFs, as well as the effect of miR-21-5p mimic on activation of the PI3K/AKT and ERK1/2 signaling pathways and the enhanced expression of pro-angiogenic (VEGF and HIF-1α) and pro-fibrogenic (PDGFRα and bFGF) genes e (Figure 6E), were all prevented by transfection with pcDNA-SPRY2. As a result of a series of rescue experiments, we have demonstrated that pcDNA-SPRY2 in HUVECs and HSFs can abolish the promoting effect of exosomal miR-21-5p mimic on angiogenesis and fibroblast function. Therefore, we concluded that exosomal miR-21-5p promoted HUVEC/HSF proliferation, angiogenesis and migration by targeting SPRY2 (Figure 6F).

Discussion

Exosomes can transfer messages of cells encoded in protein, lipids, mRNA and miRNA enclosed within a lipid bilayer acting in an autocrine and paracrine manner, in response to activation and stress inducing stimuli.[22] Incorporation of MNPs and SMF has been confirmed to enhance wound healing by improving fibrogenesis and angiogenesis.[16] In order to further improve the paracrine activities of BMSC-Exos for accelerating wound healing, we successfully fabricated a novel exosome, mag-BMSC-Exo, to transmit the stimulatory effects of MNPs and and SMF with only very little residual Fe_3O_4 nanoparticles (7.48nmol/mL) in this study.

Fibroblasts, presenting from the late inflammatory phase until full epithelialization, are critical in the processes of wound healing.[23,24] They are summoned to migrate to the wound area and proliferate to participate in wound contraction, extracellular matrix deposition, tissue remodeling, and so on.[25,26] Previous studies have proven that exosomes derived from mesenchymal stem cells (MSCs) can be internalized to regulate the proliferation and migration of fibroblasts.[27–29] In this study, mag-BMSC-Exos are demonstrated to be more conducive to enter into HSFs to improve cell migration, proliferation and expression of pro-fibrogenic genes compared with BMSC-Exos in vitro. The experiments in vivo further

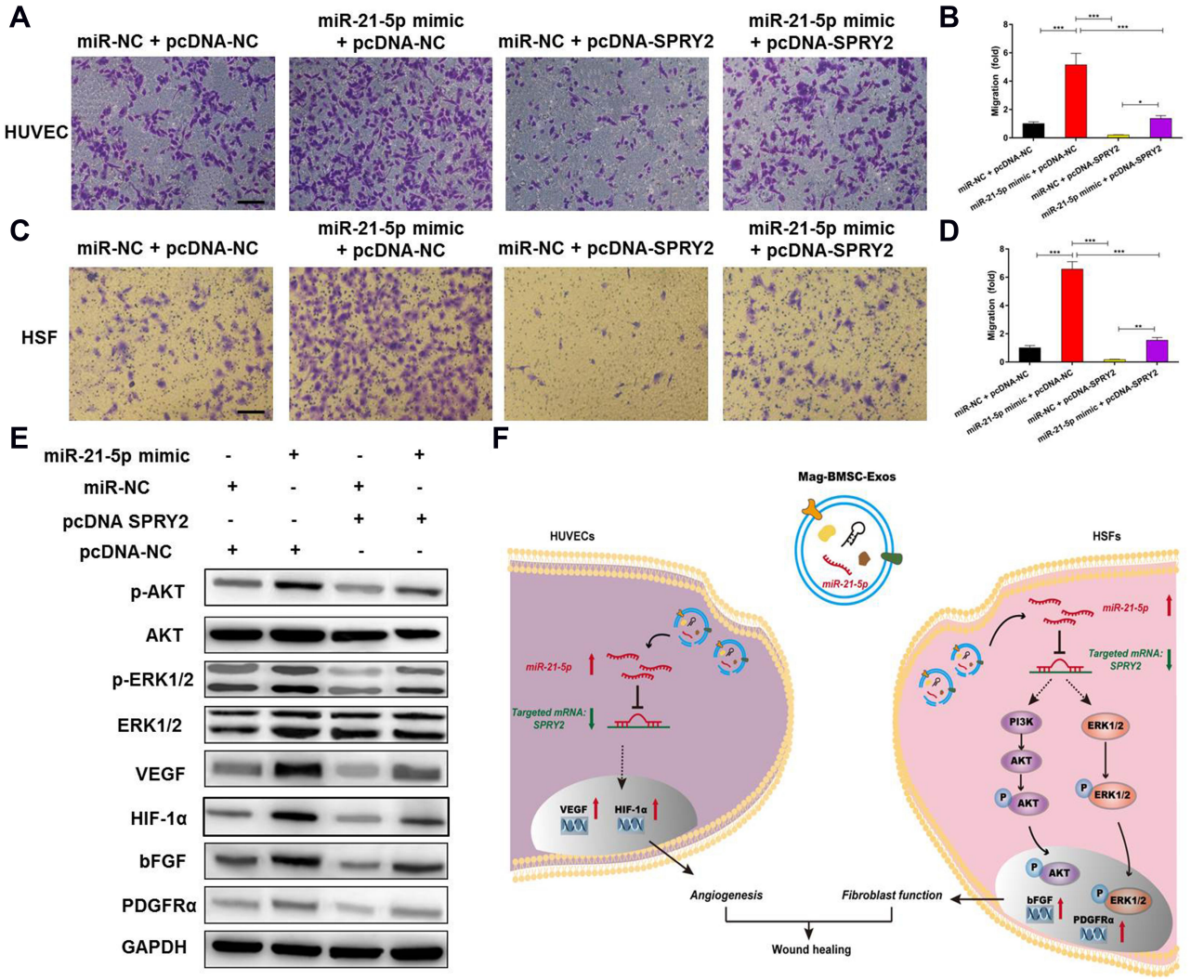

Figure 6 Exosomal miR-21-5p promotes angiogenesis and fibrogenesis by targeting SPRY2 in vitro. (*) $p < 0.05$, (**) $p < 0.01$, (***) $p < 0.001$. (**A**) Overexpression of SPRY2 prevented the upregulation of the migration rate of HUVECs induced by the miR-21-5p mimic. Scale bar = 200 μm. (**B**) Quantitative analysis of the migration rate of HUVECs. (**C**) Overexpression of SPRY2 prevented the upregulation of the migration rate of HSFs induced by the miR-21-5p mimic. Scale bar = 200 μm. (**D**) Quantitative analysis of the migration rate of HSFs. (**E**) Western blotting assays showed that overexpression of SPRY2 prevented the upregulation of AKT, p-AKT, ERK1/2 and p-ERK1/2 protein expression induced by the miR-21-5p mimic. (**F**) Schematic model showing that magnetic exosomal miR-21-5p targeted SPRY2 and activated the PI3K/AKT and ERK1/2 signaling pathways, further promoting angiogenesis and fibrogenesis.

confirmed that all these effects of mag-BMSC-Exos would enhance wound healing with a higher wound closure rate, less scar formation, and more collagen deposition in rats.

Angiogenesis, the formation of new blood vessels from the preexisting vasculature, is another essential process for wound healing.[30] As endothelial cells degrade the surrounding extracellular matrix, they begin to migrate, proliferate and interconnect to form new vessels.[4] Blood vessels move into the wound space as a unit together with macrophages and fibroblasts, and replenish nutrients and oxygen to sustain cell metabolism.[31] Furthermore, fibroblasts also can help the angiogenic process through extracellular matrix remodeling and local delivery of growth factors.[32] Exosomes from MSCs have been reported to be internalized by HUVECs and promote endothelial angiogenesis during wound repair.[27,33] Compared with BMSC-Exos, we found that mag-BMSC-Exos were more easily to be internalized by HUVECs in vitro. After that, mag-BMSC-Exos can further promote HUVECs proliferation, migration, tube formation and expression of growth factors (VEGF & HIF-1α) in vitro. All these effects of mag-BMSC-Exos were confirmed to be able to enhance wound healing with a higher wound closure rate and more new blood vessel formation in rats.

In this study, we provide the first demonstration that mag-BMSC-Exos induced prominent regenerative effects in the wound sites, as defined by a higher wound closure rate, less scar formation, more collagen deposition. We also demonstrated in vitro that mag-BMSC-Exos could be internalized into HUVECs and HSFs, activate the PI3K/AKT and ERK1/2 signaling pathways, and enhance their functional properties by transferring miR-21-5p. Our results suggest that mag-BMSC-Exos may deliver miR-21-5p into resident HUVECs and HSFs to evoke their regenerative responses, thereby accelerating cutaneous wound repair and regeneration.

To find the potential mechanism of mag-BMSC-Exos to enhance wound healing, we first conducted a miRNAs bioinformatics analysis, and found that the level of miR-21-5p was found to be up-regulated in mag-BMSC-Exos. MiR-21 is a vascular-specific member of the family of miRNA precursors that regulate angiogenesis and fibrogenesis, and miR-21 expression was found to be upregulated after skin injury and could promote keratinocyte migration to accelerate re-epithelialization of skin wounds.[34] Inhibition of miR-21 resulted in a significant delay in wound closure with less fibroblasts and collagen deposition in the wound sites, suggesting that miR-21 is a positive modulator of fibroblast function.[13,34]

Although few studies have deciphered the role of miR-21 in wound revascularization, the beneficial effects of miR-21 on endothelial cell function and tumor angiogenesis have been evaluated.[18,35] After coculturing exosomes with HUVECs and HSFs, miR-21-5p expression was remarkably enhanced in HUVECs and HSFs, which indicated that miR-21-5p can be transferred from mag-BMSC-Exos to recipient cells. These findings reveal that miR-21-5p upregulation in mag-BMSC-Exos may facilitate wound healing in this study.

To better understand the underlying mechanism of exosomal miR-21-5p to affect HUVECs and HSFs, we next employed bioinformatic tools to identify the potential target gene of miR-21-5p. We found that the gene SPRY2, which contributes to angiogenesis and fibroblast functions, was identified in different databases. Furthermore, the luciferase assay revealed that the expression of SPRY2 was increased in the miR-21-5p mimic group. It has been previously reported that the Sprouty family of proteins is a target of miR-21 in various cells and tissue types.[36] SPRY2 is an anti-angiogenic gene that can significantly inhibit cell migration and proliferation, as well as negative feedback loop modulators of the Raf/Mek/ERK-associated signaling pathways downstream of major growth factor stimuli such as FGF, VEGF, and PDGF.[37,38] In our next set of experiments, we showed that knocking down the expression of the miR-21-5p target gene SPRY2 in HUVECs and HSFs could achieve mag-BMSC-Exos-like, even miR-21-5p mimic-like, positive effects on proliferation, migration and angiogenesis. These findings suggest that miR-21-5p is one of the critical mediators in the mag-BMSC-Exo-induced regulation of processes in HUVECs and HSFs by targeting SPRY2. However, other signaling molecules may also be involved in this process, which warrants further investigation. Finally, through a series of rescue experiments, we showed that overexpression of SPRY2 in HUVECs and HSFs could attenuate, but not abolish entirely, the effects of the miR-21-5p mimic on angiogenesis and fibroblast function.

This study highlights the therapeutic potential of mag-BMSC-Exos, which may not only represent an effective and promising method for the optimization of therapeutic actions for wound healing but also act as biological vectors for the delivery of biologically functional miR-21-5p into recipient cells. However, it remains to be determined how Fe_3O_4 nanoparticles and SMF could induce BMSCs to secrete exosomes containing more miR-21-5p than BMSCs with no interventions in further studies.

Conclusions

In this study, we successfully fabricated a novel type of BMSC exosomes (mag-BMSC-Exos), in which the BMSCs were treated by Fe_3O_4 nanoparticles and SMF, can further enhance wound healing than BMSC-Exos by improving angiogenesis and fibroblast function in vitro and in vivo. Upregulation of exosomal miR-21-5p might be the potential mechanism to improve these effects by targeting SPRY2. This work offers an effective and promising protocol to improve wound healing in clinic.

Funding

This work was supported by Beijing Municipal Natural Science Foundation (7202167); Tsinghua University-Peking Union Medical College Hospital Initiative Scientific Research Program (2019ZLH209); Science Foundation for Young Scholars of Peking Union Medical College Hospital (No. pumch201912146); Fundamental Research Funds for Central Public Welfare Research Institutes, Chinese Academy of Medical Sciences (2016ZX310177-7).

Disclosure

The authors have declared that no competing interest exists.

References

1. Gravitz L. Skin. *Nature*. 2018;563(7732):S83. doi:10.1038/d41586-018-07428-4
2. Martin P. Wound healing–aiming for perfect skin regeneration. *Science*. 1997;276(5309):75–81. doi:10.1126/science.276.5309.75
3. Rodrigues M, Kosaric N, Bonham CA, Gurtner GC. Wound healing: a cellular perspective. *Physiol Rev*. 2019;99(1):665–706. doi:10.1152/physrev.00067.2017
4. Singer AJ, Clark RA. Cutaneous wound healing. *N Engl J Med*. 1999;341(10):738–746. doi:10.1056/NEJM199909023411006
5. Christenson RH. Biochemical markers of bone metabolism: an overview. *Clin Biochem*. 1997;30(8):573–593. doi:10.1016/S0009-9120(97)00113-6
6. Stappenbeck TS, Miyoshi H. The role of stromal stem cells in tissue regeneration and wound repair. *Science*. 2009;324(5935):1666–1669. doi:10.1126/science.1172687
7. Lee DE, Ayoub N, Agrawal DK. Mesenchymal stem cells and cutaneous wound healing: novel methods to increase cell delivery and therapeutic efficacy. *Stem Cell Res Ther*. 2016;7:37. doi:10.1186/s13287-016-0303-6
8. Brockelmann PJ, Muller H, Casasnovas O, et al. Risk factors and a prognostic score for survival after autologous stem-cell transplantation for relapsed or refractory Hodgkin lymphoma. *Ann Oncol*. 2017;28(6):1352–1358. doi:10.1093/annonc/mdx072
9. Sissung TM, Figg WD. Stem cell clinics: risk of proliferation. *Lancet Oncol*. 2020;21(2):205–206. doi:10.1016/S1470-2045(19)30787-9
10. Andaloussi ELS, Mager I, Breakefield XO, Wood MJ. Extracellular vesicles: biology and emerging therapeutic opportunities. *Nat Rev Drug Discov*. 2013;12(5):347–357. doi:10.1038/nrd3978
11. Yanez-Mo M, Siljander PR, Andreu Z, et al. Biological properties of extracellular vesicles and their physiological functions. *J Extracell Vesicles*. 2015;4:27066. doi:10.3402/jev.v4.27066
12. Rani S, Ritter T. The exosome - a naturally secreted nanoparticle and its application to wound healing. *Adv Mater*. 2016;28(27):5542–5552. doi:10.1002/adma.201504009
13. Hu Y, Rao SS, Wang ZX, et al. Exosomes from human umbilical cord blood accelerate cutaneous wound healing through miR-21-3p-mediated promotion of angiogenesis and fibroblast function. *Theranostics*. 2018;8(1):169–184. doi:10.7150/thno.21234
14. Li X, Wei J, Aifantis KE, et al. Current investigations into magnetic nanoparticles for biomedical applications. *J Biomed Mater Res A*. 2016;104(5):1285–1296. doi:10.1002/jbm.a.35654
15. Sapir-Lekhovitser Y, Rotenberg MY, Jopp J, Friedman G, Polyak B, Cohen S. Magnetically actuated tissue engineered scaffold: insights into mechanism of physical stimulation. *Nanoscale*. 2016;8(6):3386–3399. doi:10.1039/C5NR05500H
16. Hao S, Zhang Y, Meng J, et al. Integration of a superparamagnetic scaffold and magnetic field to enhance the wound-healing phenotype of fibroblasts. *ACS Appl Mater Interfaces*. 2018;10(27):22913–22923. doi:10.1021/acsami.8b04149
17. Imai T, Takahashi Y, Nishikawa M, et al. Macrophage-dependent clearance of systemically administered B16BL6-derived exosomes from the blood circulation in mice. *J Extracell Vesicles*. 2015;4:26238. doi:10.3402/jev.v4.26238
18. Liu Y, Luo F, Wang B, et al. STAT3-regulated exosomal miR-21 promotes angiogenesis and is involved in neoplastic processes of transformed human bronchial epithelial cells. *Cancer Lett*. 2016;370(1):125–135. doi:10.1016/j.canlet.2015.10.011
19. Li Q, Zhao H, Chen W, Huang P, Bi J. Human keratinocyte-derived microvesicle miRNA-21 promotes skin wound healing in diabetic rats through facilitating fibroblast function and angiogenesis. *Int J Biochem Cell Biol*. 2019;114:105570. doi:10.1016/j.biocel.2019.105570
20. Thum T, Gross C, Fiedler J, et al. MicroRNA-21 contributes to myocardial disease by stimulating MAP kinase signalling in fibroblasts. *Nature*. 2008;456(7224):980–984. doi:10.1038/nature07511
21. Liu LZ, Li C, Chen Q, et al. MiR-21 induced angiogenesis through AKT and ERK activation and HIF-1alpha expression. *PLoS One*. 2011;6(4):e19139. doi:10.1371/journal.pone.0019139
22. Connor DE, Paulus JA, Dabestani PJ, et al. Therapeutic potential of exosomes in rotator cuff tendon healing. *J Bone Miner Metab*. 2019;37(5):759–767. doi:10.1007/s00774-019-01013-z
23. Forrest L. Current concepts isoft connective tissue wound healing. *Br J Surg*. 1983;70(3):133–140. doi:10.1002/bjs.1800700302
24. Brainbridge P. Wound healing and the role of fibroblasts. *J Wound Care*. 2013;22(8):407–408, 410–412. doi:10.12968/jowc.2013.22.8.407
25. Diegelmann RF, Evans MC. Wound healing: an overview of acute, fibrotic and delayed healing. *Front Biosci*. 2004;9:283–289. doi:10.2741/1184
26. Schultz GS, Davidson JM, Kirsner RS, Bornstein P, Herman IM. Dynamic reciprocity in the wound microenvironment. *Wound Repair Regen*. 2011;19(2):134–148. doi:10.1111/j.1524-475X.2011.00673.x
27. Shabbir A, Cox A, Rodriguez-Menocal L, Salgado M, Van Badiavas E. Mesenchymal stem cell exosomes induce proliferation and migration of normal and chronic wound fibroblasts, and enhance angiogenesis in vitro. *Stem Cells Dev*. 2015;24(14):1635–1647. doi:10.1089/scd.2014.0316
28. Hu L, Wang J, Zhou X, et al.; Incorporating CWD, Synovium EDFM–O, Exosomes MSCPSRo. Exosomes derived from human adipose mensenchymal stem cells accelerates cutaneous wound healing via optimizing the characteristics of fibroblasts. *Sci Rep*. 2016;6:32993. doi:10.1038/srep32993

29. Kim YJ, Yoo SM, Park HH, et al. Exosomes derived from human umbilical cord blood mesenchymal stem cells stimulates rejuvenation of human skin. *Biochem Biophys Res Commun*. 2017;493(2):1102–1108. doi:10.1016/j.bbrc.2017.09.056
30. Demidova-Rice TN, Durham JT, Herman IM. Wound healing angiogenesis: innovations and challenges in acute and chronic wound healing. *Adv Wound Care (New Rochelle)*. 2012;1(1):17–22. doi:10.1089/wound.2011.0308
31. Tonnesen MG, Feng X, Clark RA. Angiogenesis in wound healing. *J Investig Dermatol Symp Proc*. 2000;5(1):40–46. doi:10.1046/j.1087-0024.2000.00014.x
32. Ucuzian AA, Gassman AA, East AT, Greisler HP. Molecular mediators of angiogenesis. *J Burn Care Res*. 2010;31(1):158–175. doi:10.1097/BCR.0b013e3181c7ed82
33. Li X, Jiang C, Zhao J. Human endothelial progenitor cells-derived exosomes accelerate cutaneous wound healing in diabetic rats by promoting endothelial function. *J Diabetes Complications*. 2016;30(6):986–992. doi:10.1016/j.jdiacomp.2016.05.009
34. Wang T, Feng Y, Sun H, et al. miR-21 regulates skin wound healing by targeting multiple aspects of the healing process. *Am J Pathol*. 2012;181(6):1911–1920. doi:10.1016/j.ajpath.2012.08.022
35. An Y, Zhao J, Nie F, et al. Exosomes from adipose-derived stem cells (ADSCs) overexpressing miR-21 promote vascularization of endothelial cells. *Sci Rep*. 2019;9(1):12861. doi:10.1038/s41598-019-49339-y
36. Zhang Y, Yuan F, Liu L, et al. The role of the miR-21/SPRY2 axis in modulating proangiogenic factors, epithelial phenotypes, and wound healing in corneal epithelial cells. *Invest Ophthalmol Vis Sci*. 2019;60(12):3854–3862. doi:10.1167/iovs.19-27013
37. Impagnatiello MA, Weitzer S, Gannon G, Compagni A, Cotten M, Christofori G. Mammalian sprouty-1 and −2 are membrane-anchored phosphoprotein inhibitors of growth factor signaling in endothelial cells. *J Cell Biol*. 2001;152(5):1087–1098. doi:10.1083/jcb.152.5.1087
38. Hanafusa H, Torii S, Yasunaga T, Nishida E. Sprouty1 and Sprouty2 provide a control mechanism for the Ras/MAPK signalling pathway. *Nat Cell Biol*. 2002;4(11):850–858.